Inkjet Printing of All Aqueous Inks to Flexible Microcapacitors for High-Energy Storage

Junjin Che, Cécile Zakri, Maxime Bronchy, Wilfrid Neri, Isabelle Ly, Philippe Poulin, Jinkai Yuan

Inkjet Printing of All Aqueous Inks to Flexible Microcapacitors for High-Energy Storage

Junjin Che, Cécile Zakri, Maxime Bronchy, Wilfrid Neri, Isabelle Ly, Philippe Poulin, Jinkai Yuan*

Univ. Bordeaux, CNRS, CRPP, UMR 5031, F-33600 Pessac, France
E-mail: jinkai.yuan@crpp.cnrs.fr

Abstract

Due to the low energy density of commercial printable dielectrics, printed capacitors occupy a significant printing area and weight in printed electronics. It has long remained challenging to develop novel dielectric materials with printability and high energy-storage density. Here, we present a novel strategy for inkjet printing of all aqueous colloidal inks to dielectric capacitors composed of carbon nanotube electrodes and polyvinylidene fluoride (PVDF)-based dielectrics. The formulated dielectric ink is composed of negatively charged PVDF latex nanoparticles complexed with cationic chitosan molecules. Beyond the isoelectric point, the PVDF@Chitosan particles demonstrate excellent printability and film-forming properties. Chitosan serves as a strong binder to improve the printed film quality yet it introduces charged species. To mitigate the transport of mobile charges, we interlayer the printed PVDF@Chitosan film with a layer of boron nitride nanosheets. This layer is perpendicular to the electric field and serves as an efficient barrier to block the transport and the avalanche of charges, eventually leading to a recoverable energy density of 15 J cm^{-3} at 610 MV m^{-1}. This energy density represents the highest value among the waterborne dielectrics. It is also superior to most of the state-of-the-art dielectric materials printed from solvent-based formulations.

1.Introduction

Low-cost and large-area printed electronics are of practical interest for emerging applications, ranging from flexible displays, sensor arrays to solar cells and energy devices.[1, 2] Printed integrated circuits (ICs) comprise a number of active components (e.g. transistors) and a larger number of passive components such as capacitors, resistors and inductors. Among them, printed capacitors form the basis of many ICs, and call for special attention due to their rich functionalities such as filtering, timing, alternating/direct current conversion, termination, decoupling, and energy storage.[3-5] Traditional film capacitors are efficient but fail to meet the needs of printed electronics due to the poor flexibility and the difficulty of soldering terminations. The ability to print dielectric materials and capacitors on planar surfaces or 3D objects is the key to realize fully printed electronics. Nevertheless, commercial printable dielectrics have still low energy densities. The printed capacitors therefore occupy a significant printing area and weight of fully printed electronics. Improving the energy density of printed capacitors is imperative to enable the reduction of size, weight, and cost of printed electronics.[6, 7]

The energy storage density U_e of dielectrics is determined by the applied electric field E and the associated electric displacement D. It can be expressed as[8, 9]

$$U_e = \int_{D_{max}}^{0} EdD \quad (1)$$

The key to improving the energy density is to achieve a high breakdown strength E_b (the maximum electric field that the material can withstand without undergoing electrical breakdown) and a large electric displacement D_{max}. So far, most of the printed capacitors have

been made by depositing droplets of ceramic nanopowder suspensions or dielectric polymer inks.[10-17] In particular, films of inorganic nanoparticles, such as $BaTiO_3$, HfO_2, and BiOCl, enjoy high polarization (high-*k*), showing an areal capacitance up to 16 nF cm^{-2},[17] but the printed ceramic films are brittle and usually need high-temperature annealing. As alternatives, polymers, such as SU-8 resin, poly(4-vinylphenol), polyimide (PI), and polydimethylsiloxane, are more appealing due to their excellent flexibility, high breakdown strength, and low losses.[12, 15, 18] However, the low dipole moments of the chemical bonds in these polymers lead to low permittivity (*k*<4), giving rise to a low energy density (~3 J cm^{-3}). Very recently, dielectric films have been printed using composite inks comprised of $Ba_{0.6}Sr_{0.4}TiO_3$ spherical particles and diverse polymers, such as poly(methyl methacrylate) (PMMA)[19, 20], or thermally induced polymerizable matrix.[21, 22] The printed dielectric films showed a high permittivity up to 55 at 1 kHz. Today, most of the developed polymeric inks need the use of large amount of harmful organic solvents. It is still a great challenge to develop highly efficient aqueous inks processed with polymers and printed to high-energy capacitors.

Colloids dispersed in aqueous solutions can be processed into solid films. They are particularly interesting for developing novel functional materials.[23-25] Among them, PVDF (polyvinylidene fluoride) latex nanoparticles, which possess high polarization (high-*k*), can be well dispersed in water thanks to the electrostatic repulsion between their negatively charged surfaces.[26, 27] Nevertheless, the stabilizing charges on the particle surface create conductive paths, induce significant leakage current, and dramatically reduce the breakdown strength of the solidified material.[27] Moreover, solution-casting pure PVDF latex usually results in poor-

quality films with cracks and voids (Figure S1, Supporting Information). They necessitate the use of diverse additives to be of better quality. The addition of insulating polyvinyl alcohol (PVA) to PVDF latex allows for isolating individual charged particles in solidified films and increasing the breakdown strength.[26] Still, the printed PVDF/PVA composite films show nanocracks as the film thickness is down to 10 μm.

Herein, we propose another strategy of using a biosourced polyelectrolyte, protonated chitosan (NH_3^+), to improve the homogeneity of printed PVDF latex film. In contrast to PVA, the cationic polyelectrolyte can electrostatically interact with surrounding latex nanoparticles and serve as a stronger binder to formulate more compact films that are free of cracks and "coffee rings" (Figure S1, Supporting Information). Furthermore, to mitigate the transport of mobile charges, a sandwich-structured composite film is printed by intercalating a nanolayer of boron nitride nanosheet (BNNS) between printed PVDF@Chitosan layers. The BNNS nanolayers perpendicular to the electric field serve as efficient barriers to block the transport of charges and improve the resistivity of printed films. To demonstrate a proof of concept, we printed microcapacitor configurations on a PI substrate. Aqueous carbon nanotube (CNT) ink is used to print the top and bottom electrodes, whereas the multi-layered dielectric film stacked between electrodes is deposited by alternately inkjet printing the PVDF@Chitosan and BNNS inks. The printed capacitor displays a high discharged energy density of 15 J cm^{-3} at 610 MV m^{-1}. To our knowledge, this energy density represents the highest value among the waterborne nanodielectrics.[26-28] The use of water makes the printing and applications of the capacitors environmentally friendly without the undesirable issues of harsh and volatile solvents.

2.Results and Discussion

Aqueous Inks and Inkjet Printing of Capacitors

CNTs are one-dimensional materials with excellent electrical conduction properties. However, it is not easy to form stable suspensions because raw CNTs tend to aggregate in the medium as a consequence of van der Waals attraction. Chitosan, a biosourced polymer, is the most abundant natural amino polysaccharide. The properties of chitosan depend largely on the degree of deacetylation. The amino group in the polymer chain makes it possible to be protonated to possess positive charges.[29] Therefore, it owns the great potential to be a bio-additive to modify the surface properties of colloids in water. In this work, chitosan was mixed with CNTs at a mass ratio of 1:1 to form a homogeneous ink (CNT@50 wt% chitosan, **Figure 1**a, e), which is used for printing conductive electrode layers.

On the other hand, water-based PVDF latex is chosen as the starting dielectric ink due to its low cost, environmental friendliness, and high permittivity. The PVDF latex dispersion (zeta potential= -30.8 mV) can remain as individual particles for years thanks to the electrostatic stabilization arising from the dissociation of the carboxylic groups on the particles (Figure 1b, f). To improve the film-forming properties, protonated chitosan solution (zeta potential= 81.5 mV) is mixed with PVDF latex so that latex particles are electrostatically complexed by chitosan molecules (Figure 1c, g). It should be noted that the chitosan dosage should be far beyond the isoelectric point (mass ratio of Chitosan/PVDF=0.8/99.2),[30] at which the zeta potential of mixture dispersions approaches 0 and the latex particles begin to flocculate and

settle. In this work, chitosan is mixed with PVDF latex at a mass ratio of 5:95 to formulate a homogeneous dielectric ink (PVDF@5 wt% chitosan) for the printing of dielectric layers.

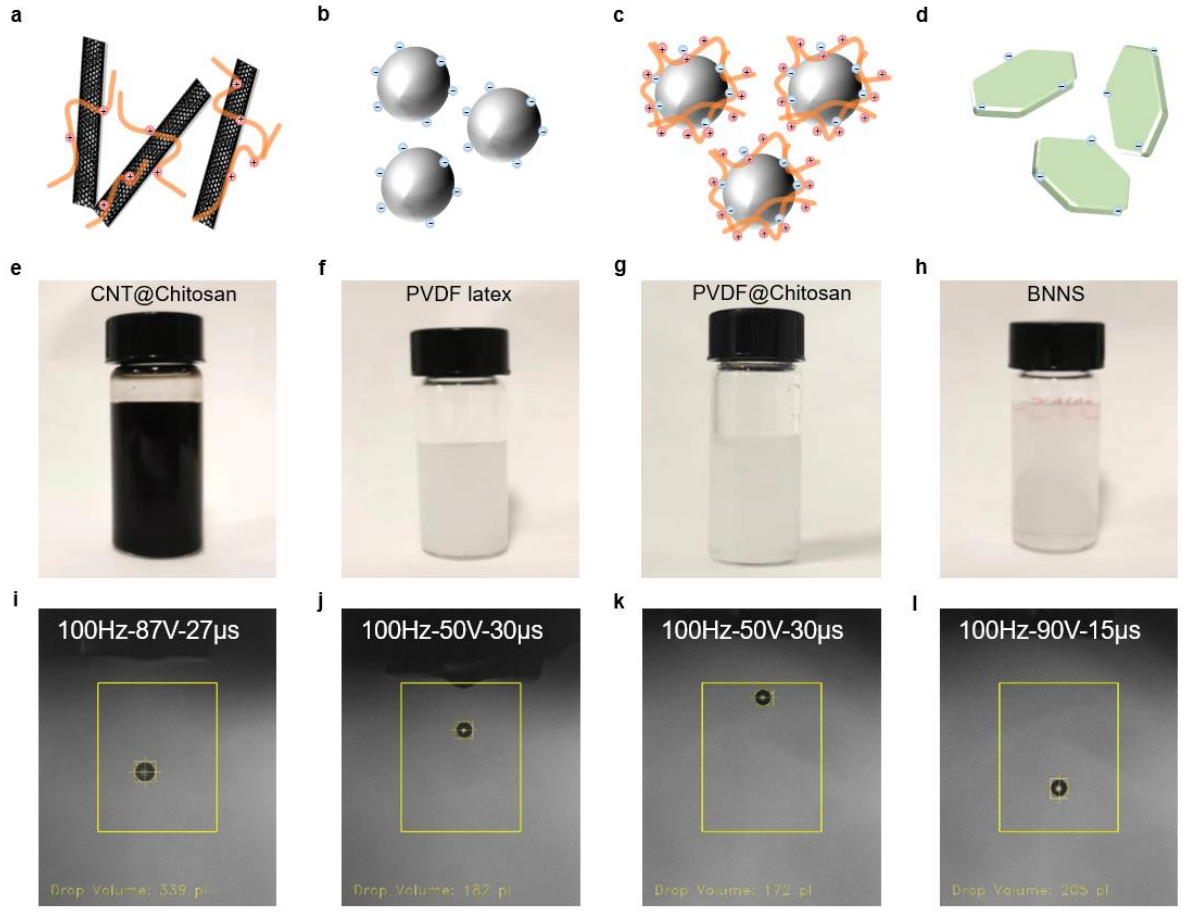

Figure 1. Schematic illustrations of the concept of aqueous inks based on different colloids: a) protonated chitosan stabilized CNTs, b) negatively charged PVDF latex, c) chitosan-coated PVDF latex particles with net positive charges, d) exfoliated BNNS nanosheets. Photographs of prepared inks: e) CNT@50 wt% chitosan ink, f) PVDF latex ink (0.77 wt%), g) PVDF@5 wt% chitosan ink (0.40 wt%), h) BNNS ink (0.035 wt%). i-l) Images of droplets generated respectively by ejecting the inks (e-h) with optimized pulse signals (frequency-applied voltage-pulse length), showing the printability of the formulated aqueous inks.

Addition of 5 wt% chitosan allows for casting a transparent, robust and defect-free PVDF latex film (Figure S1, Supporting Information). However, the PVDF@Chitosan particles

possess net positive charges (zeta potential=31.9 mV). They are surrounded by small counterions, resulting in high losses and low E_b despite of the high structural quality. To suppress these adverse effects of mobile charges, a BNNS nanolayer was intercalated in between two PVDF@Chitosan films. As 2D material, BNNS exhibits an intrinsic high breakdown strength, which scales reversely with the thickness.[5, 31-33] Aqueous BNNS ink was prepared by exfoliating BN powders in a mixture of isopropyl alcohol (IPA) and deionized water. Dispersion in pure deionized water (Figure 1d, h) was then realized by solvent exchange. The dynamic light scattering (DLS) and atomic force microscopy (AFM) image of BNNS demonstrate an average lateral size of ~460 nm and a thickness of ~30 nm (Figure S2, Supporting Information). Intriguingly, BNNS is slightly negatively charged in water (zeta potential=-21.3 mV). As a result, the nanosheets display an electrostatic affinity with PVDF@Chitosan layers, which ensures their intercalation and the homogeneity of the layer interfaces.

All the present inks are nanomaterial solutions. Uniform dispersion is the prerequisite to be ejected without clogging the microsized nozzles. The stability of inks is also critical, as printing process would take several hours and even days for industrial productions. All the inks were characterized using an optical microscopy. They are homogeneous without any sedimentation or aggregates (Figure S3, Supporting Information). Such stability can keep for up to several weeks. The stable printability of inks requires individual droplets be stably ejected without long tails and satellites. In addition to the rheological properties, the ejection of droplets is actually controlled by the management of the actuation pulse (frequency, drive voltage, and

pulse width). With optimized pulse signals (Figure 1 i-l), all the as-prepared inks (CNT@Chitosan, pure PVDF latex, PVDF@Chitosan, and BNNS dispersions) can generate high-quality droplets with a volume ranging from 170 pl to 340 pl.

The ejected droplets are deposited on a PI thin film preheated up to 130 ℃. Then a continuous line was printed by depositing suitably spaced droplets. Finally, several lines with an appropriate line distance are printed to form a macroscopic thin film. A configuration with planar parallel electrodes is used to print microcapacitors. Unlike interdigitated electrode configuration, the planar parallel electrodes, with a separation ranging from hundreds of nanometers to several micrometers, are much easier to realize, regardless of the resolution of the employed printing techniques. Such configuration significantly reduces the risk of short circuiting and generates a uniform electric field that permeates the entire volume of the material between the electrodes. The microcapacitor can be fabricated by sequentially printing well-designed patterns of the bottom electrode layer, the dielectric layer, and the top electrode layer (**Figure 2**). In detail, two layers of CNT@50 wt% chitosan inks were printed on the PI substrate to serve as the bottom electrode. After drying, nine layers of pure PVDF latex were deposited to cover the bottom electrode to serve as the middle dielectric layer. In inkjet printing of pure PVDF latex, as water evaporates, the printed film tends to crack and release the transverse tensile stresses.[26] Nevertheless, we found that subsequent printing layers can fill the cracks of previous layers. To achieve a critical thickness of ~10 μm[26], which results in high-quality PVDF latex films with fewer defects and the ability to isolate two electrodes, a minimum of nine printing layers is required. We have also found that the addition of chitosan reduces the

required number of printing layers to achieve high-quality PVDF@Chitosan films. For PVDF@5wt% chitosan ink, nine printing layers were applied to ensure that the capacitors produced had the similar active thickness. Finally, two layers of CNT@50 wt% chitosan inks were printed to serve as top electrode and form Capacitor I. In addition, to formulate a 2-2 composite structure (polymer/BNNS/polymer) in the dielectric layer, six layers of BNNS ink were printed in between two pure PVDF latex layers or PVDF@Chitosan layers before the deposition of top electrodes to form Capacitor II. All the printed capacitors were fully dried in a vacuum oven at 100 ℃ overnight before the dielectric characterizations.

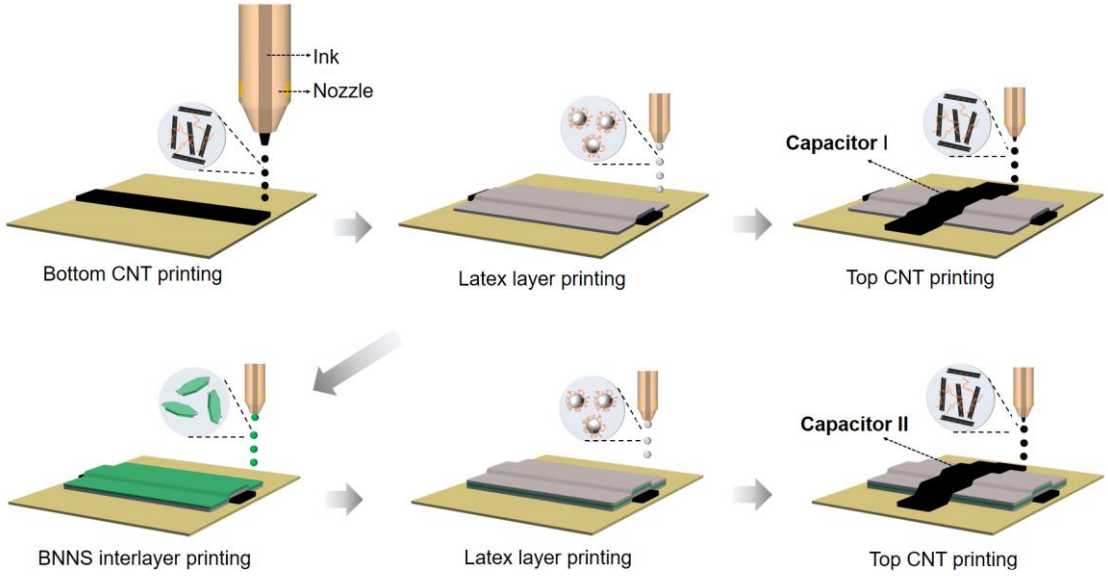

Figure 2. The inkjet printing of single-layer based dielectric Capacitor I and sandwiched-layer based Capacitor II from all aqueous functional inks.

Morphologies of Printed Capacitors

The morphologies of inkjet printed capacitors are shown in **Figure 3**. The printed CNT electrode film is 1 mm in width and ~500 nm in thickness (Figure 3a). CNTs form a 3D conductive network structure in the electrode layer (Figure 3b). This bottom CNT electrode was

fully covered by a PVDF@Chitosan dielectric layer which is geometrically wider, optically transparent, and free of defects (Figure 3c). It is noted that the CNTs in the bottom electrode layer retain the formed network structure and does not redisperse in the followed deposited PVDF inks, which is evidenced by the unchanged electrode morphology and integrity (Figure 3d). Figure 3e shows fully inkjet-printed capacitors (intersection region) with two electrodes lines (for electrical contact) and one dielectric layer in between. These inkjet-printed capacitors are fully flexible and robust, as demonstrated in Figure 3f.

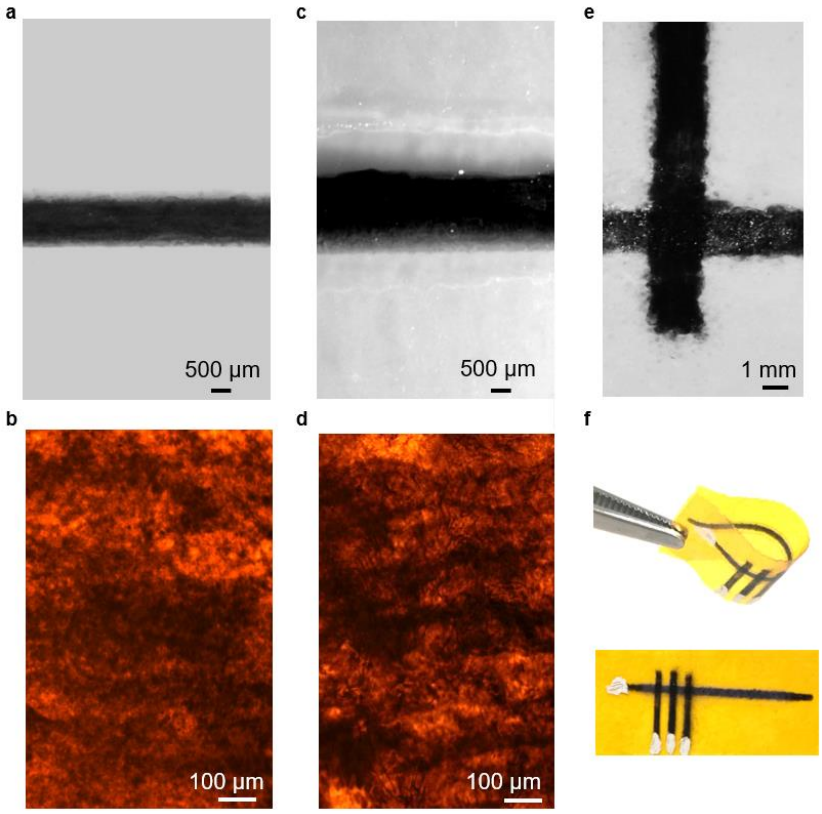

Figure 3. Optical microscope images of inkjet-printed CNT electrode under a) low magnification and b) high magnification. c, d) Optical microscope images of the bottom CNT electrode covered by a wider dielectric layer of PVDF@Chitosan. e) Optical microscope image and f) photos of flexible printed capacitors that are realized by printing a top electrode on the previously formulated PVDF@Chitosan layer in c).

The surface morphologies of the printed PVDF@Chitosan layers was also compared with that of deposited pure PVDF latex on the PI substrate. **Figure 4**a reveals the poor quality of pure PVDF latex films that are rough and full of cracks. On the contrary, when 5 wt% chitosan is introduced, the quality of the printed film is drastically improved (Figure 4b), showing a smoother surface without cracks. It should be noted that, on both films, the slight scratch and dark points are the structural defects on the surface of PI substrate pretreated in NaOH solution. To investigate the origin of the surface roughness, we printed a single layer of each ink on glass and performed AFM to visualize the surface topology. As shown in Figure S4 (Supporting Information), PVDF latex droplets demonstrated significant "coffee ring" effect. The dispersed materials are carried from the center to the edge by the Marangoni flow caused by droplet evaporation, resulting in a large height difference (root mean square deviation, Rq=146 nm), especially at the intersection of neighboring droplet edges. In addition, cracks were also found at the edges of solidified droplets. However, when 5wt% chitosan was added, the topography of the printed film became more uniform. The ring stains were significantly weakened, reducing the height difference (Rq=32 nm). Similar tendency was found for the inkjet printing of CNT inks, which were stabilized by chitosan as well. Furthermore, topographical uniformity was also observed for printed BNNS layers due to the low concentration of inks. These findings suggest that the roughness of printed patterns can be minimized by reducing coffee ring stains, optimizing droplet spacing, or using low concentration inks.

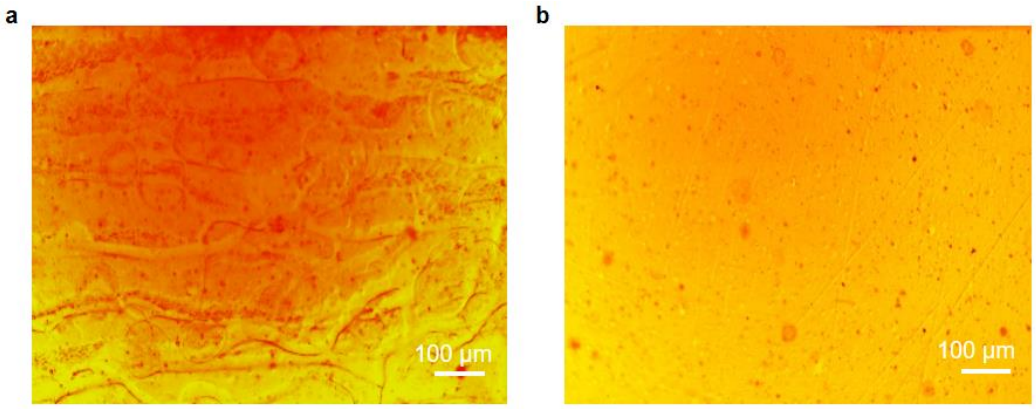

Figure 4. Optical microscope images of inkjet-printed a) pure PVDF latex film and b) PVDF@Chitosan film.

The cross-sectional scanning electron microscope (SEM) images reveal the inner structure of the inkjet-printed films. As shown in **Figure 5**a, the latex particles partially coalesced. While PVDF nanoparticles can be still identified in the PVDF@Chitosan film (Figure 5b). In the latter case, the chitosan molecules wrapped around the PVDF latex particles prevent their coalescence but still bind them together to form a closely packed film. Such organization is confirmed by the transmission electron microscopy (TEM) of printed PVDF@Chitosan films interlayered by a BNNS nanolayer (Figure 5c). Particular attention should be paid to the layer interfaces as printing heterostructures, which usually suffer greatly from the redispersion of materials as printing subsequent layers. It is noted that a continuous and compact BNNS nanolayer was formed without apparent cracks or defects between BNNS and polymer, indicating excellent layer affinity and compatibility. This is actually driven by the electrostatic attraction between negatively charged BNNS and positively charged PVDF@Chitosan particles. Furthermore, the absence of voids and delamination reflects the good affinity of the CNT electrodes with their neighbouring layers of PI substrate and PVDF@Chitosan layer (Figure 5d).

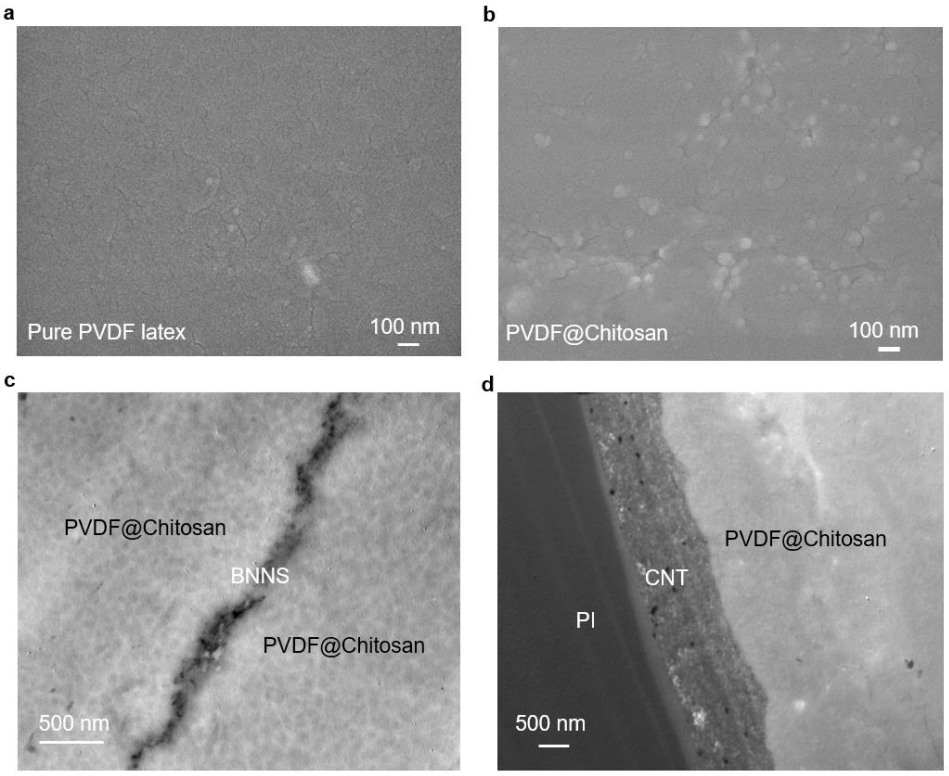

Figure 5. Cross-sectional SEM images of inkjet-printed a) PVDF latex film and b) PVDF@Chitosan film. TEM images of c) the interfaces between the inkjet-printed BNNS layer and PVDF@Chitosan layers and d) layer interfaces between the CNT electrode layer and PVDF@Chitosan layer and PI substrate.

To further demonstrate the mechanical robustness of the layer interfaces, we performed cyclical bending tests on a 33.5 mm long printed sandwiched sample by applying a maximum displacement of 7 mm over 100 cycles (**Figure 6**a). Subsequently, we used SEM at various magnifications to examine the interfaces between the PI, CNT, PVDF@Chitosan, and BNNS layers. The results, shown in Figure 6 b-d, reveal no discernible signs of holes or phase separation at the interfaces.

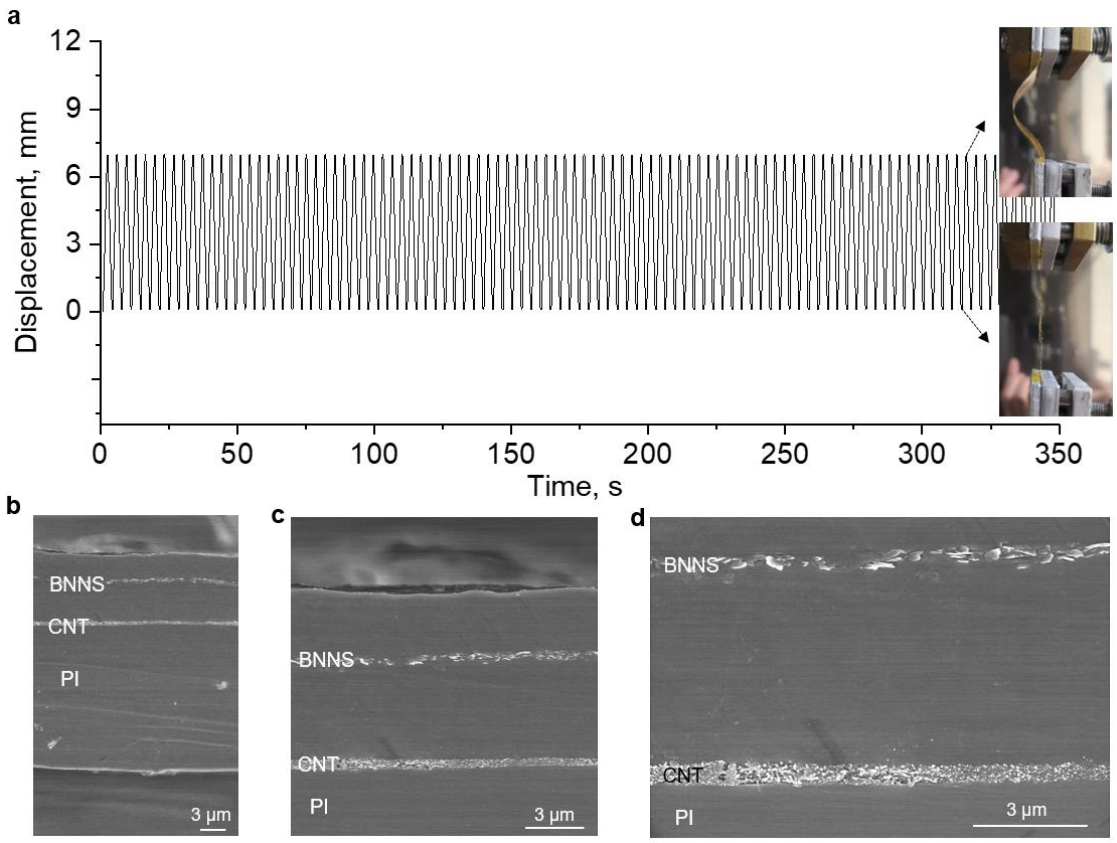

Figure 6. a) Mechanical bending deformation applied on the printed sandwiched PVDF@Chitosan composite film over 100 cycles. b-d) SEM images of the layer interfaces between the PI, CNT, PVDF@Chitosan, and BNNS layers.

Dielectric Performances of Inkjet-Printed Capacitors

An efficient printed capacitor necessitates a highly conductive printed electrode. In our study, the anisotropic CNTs contact each other and form 3D conductive networks, leading to high conductivity. A maximum conductivity (5500 S m^{-1}) was achieved in CNT film with uniform morphologies printed with optimized printing parameters, i.e., drop spacing of 60 μm and two printing passages (Figure S5, Supporting Information). The capacitive behaviours of the printed capacitors are characterized by impedance spectroscopy. **Figure 7**a shows the permittivity of printed dielectrics as a function of frequency. The coalesced PVDF latex film displays a drop of apparent permittivity at low frequency. This arises from the polarization of

the electrodes and the formation of an electric double layer at their surface. Such electrode polarization depends on the electrode surface properties and ion concentrations in the medium. Due to the presence of free charges and electrode polarization, the apparent permittivity is higher than that of typical PVDF films (k~10).[34, 35] In parallel, these free charges also contribute to the conductivity, which is evidenced by the increment in AC conductivity and losses (Figure 7b,c). The conduction of these free charges is however determined by their transport dynamics and the nature of medium.

The addition of chitosan weakens the electrode polarization and leads to a decreased permittivity in the entire frequency range. Meanwhile the conductivity is decreased and the losses are suppressed. Unfortunately, the ion-associated electrode polarization still exists in PVDF@Chitosan films at frequencies below 100 Hz because of the presence of the counterions attracted by the slightly positively charged PVDF@Chitosan particles. However, when both films are interlayered by BNNS, the overall conductivity, and dielectric losses are largely reduced. It should be noted that such a small amount of BNNS should not change the intrinsic permittivity of composite films. However, the measured permittivity involves the contribution of electrode polarization. Even a small amount of BNNS can change the apparent permittivity by changing the concentration of free charges in the material.[30] However, the printed pure latex film has a rough surface full of structural defects (Figure 4a and Figure S4, Supporting Information). This material is not ideal to serve as substrate for subsequent printing of a compact BNNS nanolayer. Nevertheless, chitosan has excellent film forming properties. It electrostatically interacts with PVDF nanoparticles and serve as a stronger binder to formulate

more compact substrate that are smooth and free of defects (Figure 4b, Figure S4, Supporting Information), enabling printing of more compact and uniform BNNS layers on it. The improved insulating properties of the interlayered PVDF@Chitosan system can potentially give rise to higher energy storage performances.

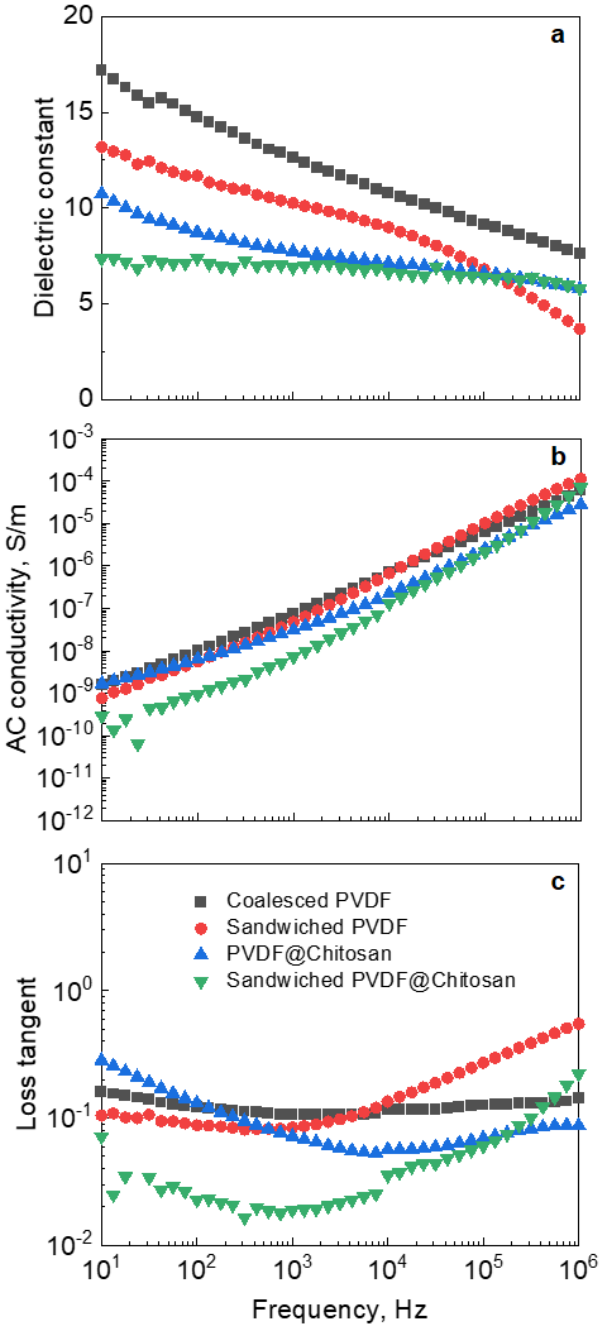

Figure 7. a) Dielectric constant, b) AC conductivity, and c) loss tangent of printed films as a function of frequency at room temperature.

Energy Storage Performances of Fully Inkjet-printed Capacitors

We first evaluate the maximum electric field that the printed capacitors can sustain before dielectric failure. The measured breakdown strength E was analysed using the Weibull distribution function:[36, 37]

$$P(E) = 1 - e^{-\left(\frac{E}{E_b}\right)^{\beta}} \quad (2)$$

where $P(E)$ is the cumulative probability of dielectric failure, E_b is the characteristic breakdown strength that corresponds to ~63.2% probability of failure, and β is the so-called shape parameter that describes the uniformity of the printed films. As shown in **Figure 8**, the addition of 5 wt% chitosan improves the E_b from 204 MV m^{-1} to 271 MV m^{-1} by improving the film quality and suppressing morphological defects (cracks). However, the films still have inferior E_b as compared to that (>350 MV m^{-1}) of typically solution-or melt-processed PVDF films[38-41] because of the presence of charged species. Interestingly, the sandwiched films show significantly improved E_b compared to the pristine films, namely from 387 MV m^{-1} for the PVDF/BNNS/PVDF film to 587 MV m^{-1} for the PVDF@Chitosan/BNNS/PVDF@Chitosan film. To reveal the origin of the improved E_b, we measured the resistivity of the printed films at high fields until their breakdown strength and plotted the results in Figure S6 (Supporting Information). It is found that all the films demonstrate a nonlinear conduction behavior at high fields. Intriguingly, at the same field, sandwiched materials exhibit higher resistivity than their counterparts, showing the charge carrier blockage effect of BNNS interlayers.[42-44] Sandwiched PVDF@Chitosan demonstrated the highest resistivity, which is responsible for the high breakdown strength.

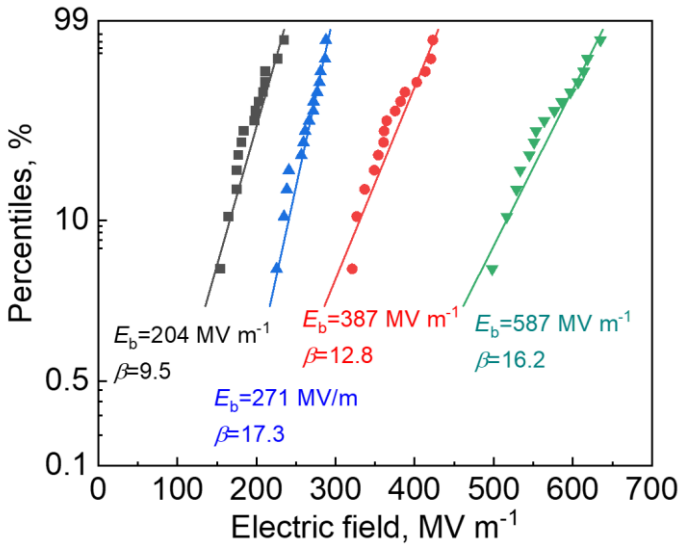

Figure 8. Weibull distribution of measured dielectric breakdown strength for different printed films: from left to right, pure PVDF latex film (black), PVDF@Chitosan film (blue), pure latex film interlayered by BNNS (red), BNNS intercalated PVDF@Chitosan film (green). The E_b and shape factor β are listed below the cure for each film.

The high E_b is favorable to achieve a high energy-storage density. We characterized the polarization and energy storage density of inkjet printed capacitors at high electric fields. The polarization-electric field (*P*-*E*) loops were first measured at 200 MV m^{-1}, which is close to the E_b of coalesced PVDF latex films. As shown in **Figure 9**a, the variation of maximum polarization P_{max} demonstrates the same trend as that of permittivity (Figure 7a). The sandwiched PVDF@Chitosan layer displays the lowest value. However, its *P*-*E* loop is much slimmer than its counterparts, showing dramatically reduced conduction losses at high fields as a consequence of the strong constrain effect of BNNS on the movement of free charge carriers. It is particularly interesting to investigate the polarization of the sandwiched PVDF@Chitosan films at higher electric fields near its breakdown strength. As shown in Figure 9b, the P_{max} increases with the electric field, yet the composites show larger losses and thus a higher remnant

polarization P_r at higher fields. The discharged energy density is then calculated and compared with other printed films. As shown in Figure 9c, the pure PVDF and PVDF@Chitosan films exhibit discharged energy densities of 2.3 J cm^{-3} and 4.3 J cm^{-3} respectively, both of which are lower than the sandwich-structured films. The PVDF/BNNS/PVDF film has an energy density of 9.4 J cm^{-3} while PVDF@Chitosan/BNNS/PVDF@Chitosan film shows a maximum value of 15 J cm^{-3}. To the best of our knowledge, this energy density represents the highest value among the waterborne nanodielectrics.[26-28, 30]. Additionally, cyclic charge/discharge were tested on sandwiched PVDF@Chitosan films over 10^4 cycles under 100 MV m^{-1} (Figure S7, Supporting Information). No sign of aging was found, indicating the long-term stability of the energy storage performances of printed microcapacitors. It should be noted that chitosan contains various reactive functional groups, such as amino, primary and secondary hydroxyl groups. The PVDF@Chitosan layer that comes into direct contact with the electrodes may undergo chemical modification through redox reactions. However, the medium remains insulating, and the chitosan in the bulk is not chemically modified.[30] The aging test at high fields (Figure S7, Supporting Information) did not indicate any signs of chemical degradation. To minimize the potential influence of redox reactions on energy storage performance at high fields, increasing the printing layer thickness can be a viable option.

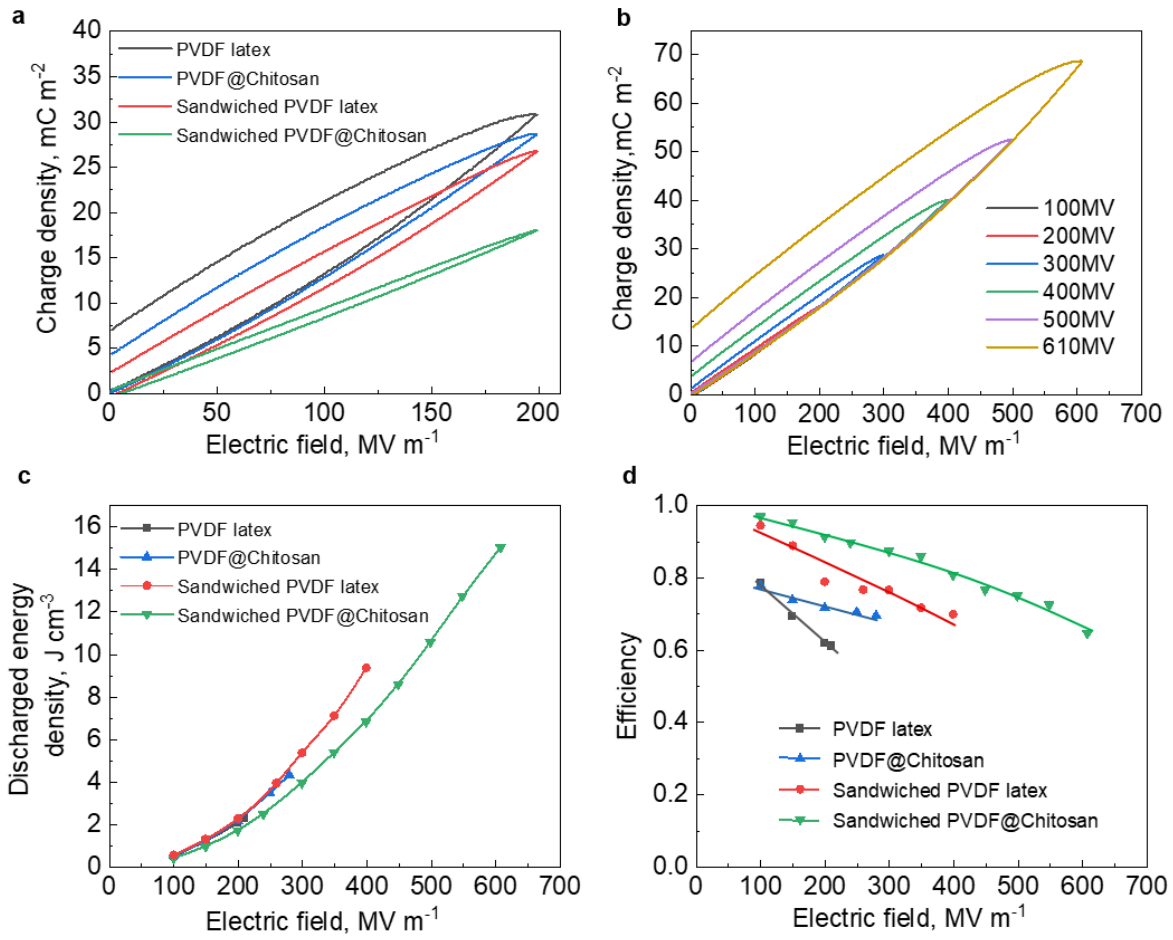

Figure 9. a) *P-E* loops of inkjet-printed dielectric films at 200 MV m^{-1}. b) *P-E* loops of the sandwiched PVDF@Chitosan composite films at different electric fields. c) The discharged energy density and d) charge/discharge efficiency as a function of the electric field for inkjet-printed films.

In addition to the energy density, it is also critical to evaluate the charge/discharge efficiency η, which is defined as the ratio of recoverable energy and charged energy. As shown in Figure 9d, the efficiency decreases with the applied field due to the conduction losses at high fields. It is noted that the introduction of chitosan and particularly BNNS nanolayers enhance the efficiency, which is another proof of the film's quality improvement as a result of the chitosan incorporation as well as the ability of BNNS to improve resistivity and to decrease conduction losses.

Table 1 compares the dielectric properties of sandwiched PVDF@Chitosan films with the state-of-the-art inkjet printed materials. So far, most of the printed capacitors have been realized by inkjet-depositing droplets of ceramic nanopowder suspensions or polymer dielectric inks. Their capacitive energy storage performances are limited and most of the ink formulations are based on environmentally problematic solvent processes. In contrast, our work relies on all aqueous functional inks to inkjet print layer-by-layer sandwiched dielectric layers, which not only show low losses but also demonstrate extremely high breakdown strength and energy storage properties, providing thereby a sustainable route toward next-generation printable dielectric materials.

Table 1. The formulated dielectric inks and the dielectric properties of printable materials reported in the literature.

Ink Materials	Solvent	C (nF cm^{-2})	k (@1kHz)	Tanδ	E_b (MV m^{-1})	U_e (J cm^{-3})	Ref
$BaTiO_3$/P(VDF-TrFE)[a]	Dimethylformamide	1.2	70	0.07			[7]
hBN[b]	Water	2	6.1		190	0.97	[10]
HfO_2	Mixed aliphatic compounds	27.9	12.6@1M Hz	0.0125			[11]
PVPh/PMF[c]	Hexanol-6		5	0.025	71	0.11	[12]
SU-8	Cyclopentanone	3.6	3@100 Hz	0.04	14	0.003	[12]
BiOCl	IPA	16.6	>40		67	0.79	[17]
PMMA/66 vol%$BaSrO_3$	Butanone		~50@100 Hz	~0.14			[19]
PMMA/BST[d]	Butanone		28	0.043			[20]
BST	BDG and IPA	85.5	43@ 200kHz	0.15			[22]
PVDF/PVA	Water	46	10	0.06	550	12.0	[26]
PMMA/82 wt% CNO[e]	Acetone		8.5	0.12			[45]
SiO_2	Anhydrous xylene and ethanol		4.1	0.08			[46]
PTD[f]	Diisopropenylbenzene and 2,4,6-triallyloxy-1,3,5-triazene		13	0.1	767.4	32.0	[47]
2,4,6-triallyoxy-1,3,5-triazine (TOTZ, T)]	BPMA[i]	4	3@100Hz	0.04	200	0.53	[48]
PEDOT[h]	Poly(biphenyltetracarboxylic dianhydride-co-phenylenediamine)	13	0.5@3MHz				[49]
$ZrSiO_4$	Anhydrous xylene/ethanol		5.1	0.075			[50]
$BaTiO_3$/Resin	N, N-dimethylformamide	44	75@1MHz	0.011			[51]
PVDF@Chitosan	Water	3.28	7.39	0.023	610	15.0	This work

[a]Poly(vinylidene fluoride-trifluoroethylene). [b]Hexagonal boron nitride. [c]Poly(4-vinylphenol)/poly(melamineco-formaldehyde). [d]$Ba_{0.6}Sr_{0.4}TiO_3$. [e]$Ca_2Nb_3O_{10}$. [f][pentaerythritol tetrakis(3-meracproprinate) (PEMP, P), 1,3-diisopropenylbenzene (DPB, D), 2,4,6-triallyoxy-1,3,5-triazine (TOTZ, T)]. [h]Poly(3,4-ethylenedioxythiophene)-poly(styrenesulfonate). [i]4-benzoylphenyl methacrylate

Note: The energy density values U_e that are not recorded in refs are estimated according to $U_e = 1/2\varepsilon_0\varepsilon_r E_b^2$, where ε_r is the relative permittivity, and ε_0 is the permittivity of free space (=8.85 × 10^{-12} F m^{-1}).

3.Conclusions

We have inkjet-printed capacitors with high energy density and high efficiency by using environmentally friendly functional inks: conductive CNT inks, dielectric PVDF-based inks, and BNNS inks. These inks are formulated in water, fully inkjet printable and allow for the formation of stable droplets of several hundred pl in volume. The introduction of chitosan results in the formation of higher-quality dielectric films free of defects as compared to pure PVDF latex films, leading to an improved breakdown strength. Moreover, it was shown that the printed BNNS interlayers largely improve the resistivity as an efficient barrier at high fields. The printed sandwiched layer demonstrates significantly improved breakdown strength and energy storage density. This principle is validated for both pure PVDF and PVDF@Chitosan sandwich structures. Because of the structural uniformity, the latter shows the greatest energy density of 15 J cm^{-3} at 610 MV m^{-1}. It is anticipated that this work opens a promising route for the realization of environmentally benign inks and the printing of high-energy flexible dielectric capacitors.

4.Experimental Section

Materials: CNTs were supplied by Nanocyl under the series name of NANOCYL NC3100. PVDF latex was provided by Arkema (Kynar Aquatec ARC Latex) with an initial concentration of solid content of 44 wt%. In the latex nanoparticles, the ratio between the fluoropolymer and acrylic resin is 70:30. Such PVDF latex is found in amorphous phase (Figure S8, Supporting Information). Chitosan was supplied by Sigma-Aldrich (from crab shells, 85% deacetylated). Hexagonal BN powder was purchased from Merck KGaA, Germany, which has a platelet

thickness of ~ 1 μm. IPA (Isopropyl alcohol) was supplied by Sigma-Aldrich (2-Propanol, suitable for HPLC, 99.9%). Sodium hydroxide was supplied by Sigma-Aldrich.

Ink Preparation: The PVDF ink was obtained by diluting the received PVDF latex with deionized water to a concentration of 0.77 wt%. Protonated chitosan was prepared by dissolving chitosan pellets in an aqueous solution with 1.5 wt% acetic acids.[29,30] The obtained protonated chitosan solution was diluted to a concentration of 0.75 wt% for use after. To prepare conductive CNT ink, CNT powders were first dispersed in deionized water at 2 wt%. The solution was magnetically stirred at room temperature for 2 h. Then it was mixed with the chitosan solution and deionized water to reach a CNT/Chitosan mass ratio of 1:1 at 0.25 wt% of each. The mixture solution was magnetically stirred and then tip sonicated for 30 min. Afterward, it was centrifuged at 2486 g for 30 min and filtered with a 5 μm filter to obtain a well-dispersed ink without aggregates. The final solute concentration was remeasured at 0.4794 wt%, and 0.2397 wt% for CNT and chitosan respectively. This ink is referred to CNT@50 wt% chitosan. Similarly, the PVDF@Chitosan aqueous inks were prepared by mixing different quantities of 0.77 wt% PVDF latex, 0.75 wt% chitosan, and deionized water to achieve an ink composed of 0.38 wt% PVDF/0.02 wt% chitosan. The final ink was diluted to a concentration of 0.4 wt% solutes by adding deionized water. The ink is referred to PVDF@5 wt% chitosan. Furthermore, following the well-established protocols of the liquid phase exfoliation process,[52] the BN powder was dispersed and exfoliated in a 1:1 co-solution of IPA and deionized water. The solution was magnetically stirred and then tip-sonicated. Then it was centrifuged at 10000 g for 30 min to remove the thick unexfoliated platelets. Afterward, the

supernatant was centrifuged at 30000 g for 30 min to collect the exfoliated flakes. The collected BN flakes were redispersed in water by tip sonication. Such solvent exchange was applied and repeated three times. Finally, the obtained solution was filtered with a 5 μm filter. The final concentration of prepared ink was remeasured at 0.035 wt%.

Inkjet Printing: An inkjet printer (Autodrop compact microdispensing system MD-P-82x) with a nozzle of 100 μm diameter was used for printing microcapacitors. In the nozzle unit, a piezoelectric actuator controls the pressure variation and generates ink droplets on demand. The applied pulse signal can be adjusted to control the droplet properties by tuning the applied voltage, pulse length, and frequency. The ejected droplets and the required pulse signal for the droplet generation were listed as follows. 87 V of pulse voltage and 27 μs of pulse length at an ejection frequency of 100 Hz were chosen to produce CNT@50 wt% chitosan ink droplets of typical volume between 100 pl and 400 pl. A drop spacing of 60 μm was utilized for the printing of electrodes. The PVDF latex ink and PVDF@5 wt% chitosan aqueous ink were ejected by using 50 V of pulse voltage and 30 μs of pulse length at an ejection frequency of 100 Hz. A drop spacing of 50 μm is set for the printing of the dielectric layers. Droplets of BNNS aqueous ink were generated with 90 V of pulse voltage and 15 μs of pulse length at an ejection frequency of 100 Hz.

Characterizations: The optical microscope images of dispersions of colloidal inks were examined with Leica DM 2500P. The TEM image of the BNNS was obtained with Hitachi H7650 operating at 80 kV. AFM images of BNNS and printed films were taken in dry condition and captured with a Dimension ICON (Veeco, Bruker) at a scan rate of 1 Hz in tapping mode.

Samples were obtained by a spin coating of diluted ink on silicon substrates and by single passage inkjet printing on glass for BNNS and printed films respectively. The size and the surface charges of the nanoparticles in the prepared inks were measured using Malvern Zetasizer Nano at 20 ℃. The surface morphology of the printed films was studied by microscopic observation under an optical microscope (Leica DM 2500P) with ×10 and ×40 objectives. The cross-sectional SEM image of the printed films was obtained by JEOL 6700F. The TEM images were taken via a Hitachi H600 microscope. The samples are ultramicrotomized into 40-60 nm thick slices using a cryo ultramicrotome (Leica UC7). The dielectric properties of the printed samples were measured as a function of frequency from 10 to 10^6 Hz at room temperature using an impedance analyzer (MaterialsMates 7260, Italia). A PolyK ferroelectric polarization loop and dielectric breakdown system were used for the characterizations of dielectric breakdown strength, high-field resistivity, cyclic charge/discharge aging, and electric polarization-electric field loops at 100 Hz.

Supporting Information

Supporting Information is available from the Wiley Online Library or from the author.

Acknowledgments

This research is supported by the ANR project 3Dielectric (ANR-21-CE06-0001-01). This study also received financial support from the French government in the framework of the University of Bordeaux's IdEx "Investments for the Future" program/GPR PPM. Dr. Che would like to acknowledge the Chinese Scholarship Council. All authors are grateful to Kyriaki Samioti for her assistance on the dielectric characterizations, and to Gilles Pecastaings for the

AFM characterizations. Arkema is also gratefully acknowledged for the donation of PVDF materials.

Conflict of Interest

The authors declare no conflict of interest.

Data Availability Statement

The data that supporting the findings of this study are available from the corresponding author upon reasonable request.

Keywords

Inkjet printing, aqueous inks, energy storage density, dielectrics, polymer composites

Received: ((will be filled in by the editorial staff))

Revised: ((will be filled in by the editorial staff))

Published online: ((will be filled in by the editorial staff))

References

[1] M. Gao, L. H. Li, Y. L. Song, *J. Mater. Chem. C* **2017**, 5, 2971.

[2] S. Chung, K. Cho, T. Lee, *Adv. Sci.* **2019**, 6, 1801445.

[3] Z. M. Dang, J. K. Yuan, J. W. Zha, T. Zhou, S. T. Li, G. H. Hu, *Prog. Mater. Sci.* **2012**, 57, 660.

[4] X. D. Wu, X. Chen, Q. M. Zhang, D. Q. Tan, *Energy Stor. Mater.* **2022**, 44, 29.

[5] Q. Li, L. Chen, M. R. Gadinski, S. H. Zhang, G. Z. Zhang, H. Y. Li, A. Haque, L. Q. Chen, T. N. Jackson, Q. Wang, *Nature* **2015**, 523, 576.

[6] Y. Khan, A. Thielens, S. Muin, J. Ting, C. Baumbauer, A. C. Arias, *Adv. Mater.* **2020**, 32, 1905279.

[7] T. Siponkoski, M. Nelo, J. Perantie, J. Juuti, H. Jantunen, *Compos. B. Eng.* **2015**, 70, 201.

[8] Z. M. Dang, J. K. Yuan, S. H. Yao, R. J. Liao, *Adv. Mater.* **2013**, 25, 6334.

[9] B. Yang, Y. Zhang, H. Pan, W. Si, Q. Zhang, Z. Shen, Y. Yu, S. Lan, F. Meng, Y. Liu, H. Huang, J. He, L. Gu, S. Zhang, L. Q. Chen, J. Zhu, C. W. Nan, Y. H. Lin, *Nat. Mater.* **2022**, 9,1074.

[10] R. Worsley, L. Pimpolari, D. McManus, N. Ge, R. Ionescu, J. A. Wittkopf, A. Alieva, G. Basso, M. Macucci, G. Iannaccone, K. S. Novoselov, H. Holder, G. Fiori, C. Casiraghi, *ACS Nano* **2019**, 13, 54.

[11] G. Vescio, J. Lopez-Vidrier, R. Leghrib, A. Cornet, A. Cirera, *J. Mater. Chem. C* **2016**, 4, 1804.

[12] B. K. Tehrani, C. Mariotti, B. S. Cook, L. Roselli, M. M. Tentzeris, *Org. Electron.* **2016**, 29, 135.

[13] A. Matavz, B. Malic, V. Bobnar, *J. Appl. Phys.* **2017**, 122, 214102.

[14] X. Ding, Y. X. Li, D. Wang, Q. R. Yin, *Ceram. Int.* **2004**, 30, 1885.

[15] F. Zhang, C. Tuck, R. Hague, Y. F. He, E. Saleh, Y. Li, C. Sturgess, R. Wildman, *J. Appl. Polym. Sci.* **2016**, 133, 43361.

[16] A. G. Kelly, D. Finn, A. Harvey, T. Hallam, J. N. Coleman, *Appl. Phys. Lett.* **2016**, 109, 023107.

[17] Y. Nalawade, J. Pepper, A. Harvey, A. Griffin, D. Caffrey, A. G. Kelly, J. N. Coleman, *ACS Appl. Electron. Mater.* **2020**, 2, 3233.

[18] R. Mikkonen, P. Puistola, I. Jönkkäri, M. Mäntysalo, *ACS Appl. Mater. Interfaces.* **2020**, 12, 11990.

[19] M. Mikolajek, T. Reinheimer, N. Bohn, C. Kohler, M. J. Hoffmann, J. R. Binder, *Sci. Rep.* **2019**, 9,13324.

[20] M. Mikolajek, A. Friederich, C. Kohler, M. Rosen, A. Rathjen, K. Kruger, J. R. Binder, *Adv. Eng. Mater.* **2015**, 17, 1294.

[21] T. Reinheimer, R. Azmi, J. R. Binder, *ACS Appl. Mater. Interfaces.* **2020**, 12, 2974.

[22] T. Reinheimer, V. Baumann, J. R. Binder, *Nanomaterials* **2020**, 10, 2302.

[23] J. L. Keddie, *Mater. Sci. Eng. R Rep.* **1997**, 21, 101.

[24] L. A. Renna, C. J. Boyle, T. S. Gehan, D. Venkataraman, *Macromolecules* **2015**, 48, 6353.

[25] M. A. Boles, M. Engel, D. V. Talapin, *Chem. Rev.* **2016**, 116, 11220.

[26] F. Torres-Canas, J. Yuan, I. Ly, W. Neri, A. Colin, P. Poulin, *Adv. Funct. Mater.* **2019**, 29, 1901884.

[27] J. Che, W. Neri, I. Ly, P. Poulin, C. Zakri, J. Yuan, *ACS Appl. Energy Mater.* **2020**, 3, 9107.

[28] S. M. Goodman, J. Che, W. Neri, J. Yuan, A. B. Dichiara, *Energy Stor. Mater.* **2022**, 48, 497.

[29] M. N. R. Kumar, *React. Funct. Polym.* **2000**, 46, 1.

[30] J. Che, C. Zakri, I. Ly, W. Neri, E. Laurichesse, J. P. Chapel, P. Poulin, and J. K. Yuan, *Adv. Funct. Mater.* **2023**, 2213804.

[31] B. Fan, M. Zhou, C. Zhang, J. Yuan, D. He, Y. Liu, P. Haghi-Ashtiani, J. Bai, *J. Phys. Chem. C* **2019**, 123, 11993.

[32] Y. Hattori, T. Taniguchi, K. Watanabe, K. Nagashio, *ACS Nano* **2015**, 9, 916.

[33] A. Ranjan, N. Raghavan, M. Holwill, K. Watanabe, T. Taniguchi, K. S. Novoselov, K. L. Pey, S. J. O'Shea, *ACS Appl. Electron. Mater.* **2021**, 3, 3547.

[34] J. K. Yuan, S. H. Yao, W. L. Li, A. Sylvestre, J. B. Bai, *J. Phys. Chem. C* **2017**, 121, 12063.

[35] J. K. Yuan, *Chin.* Chem. *Lett.* **2017**, 28, 2036.

[36] X. Y. Huang, B. Sun, Y. K. Zhu, S. T. Li, P. K. Jiang, *Prog. Mater. Sci.* **2019**, 100, 187.

[37] Y. Liu, J. Chen, X. Jiang, P. Jiang, X. Huang, *ACS Appl. Energy Mater.* **2020**, 3, 5198.

[38] B. H. Fan, Z. L. Xing, F. Bedoui, J. K. Yuan, X. X. Lu, D. L. He, M. Y. Zhou, C. Zhang, Z. M. Dang, S. Weigand, J. B. Bai, *Polymer* **2020**, 190,122235.

[39] W. J. Li, Q. J. Meng, Y. S. Zheng, Z. C. Zhang, W. M. Xia, Z. Xu, *Appl. Phys. Lett.* **2010**, 96, 192905.

[40] W. Xia, Z. Xu, F. Wen, W. Li, Z. Zhang, *Appl. Phys. Lett.* **2010**, 97, 222905.

[41] J. K. Yuan, Z. M. Dang, S. H. Yao, J. W. Zha, T. Zhou, S. T. Li, J. Bai, *J. Mater. Chem.* **2010**, 20, 2441.

[42] Y. K. Zhu, Y. J. Zhu, X. Y. Huang, J. Chen, Q. Li, J. L. He, P. K. Jiang, *Adv. Energy Mater.* **2019**, 9, 1901826.

[43] J. W. Yang, H. A. Xie, H. Chen, Z. Q. Shi, T. Wu, Q. L. Yang, C. X. Xiong, *J. Mater. Chem. A* **2018**, 6, 1403.

[44] F. H. Liu, Q. Li, J. Cui, Z. Y. Li, G. Yang, Y. Liu, L. J. Dong, C. X. Xiong, H. Wang, Q. Wang, *Adv. Funct. Mater.* **2017**, 27, 1606292.

[45] X. Z. Wu, F. Fei, Z. Chen, W. M. Su, Z. Cui, *Compos. Sci. Technol.* **2014**, 94, 117.

[46] J. Varghese, K. P. Surendran, M. T. Sebastian, *RSC Adv.* **2014**, 4, 47701.

[47] B. C. Riggs, R. Elupula, S. M. Grayson, D. B. Chrisey, *J. Mater. Chem. A* **2014**, 2, 17380.

[48] Y. Ge, M. Plotner, A. Berndt, A. Kumar, B. Voit, D. Pospiech, W. J. Fischer, *Semicond. Sci. Technol.* **2017**, 32, 095012.

[49] Y. Liu, T. H. Cui, K. Varahramyan, *Solid State Electron.* **2003**, 47, 1543.

[50] J. Varghese, M. Teirikangas, J. Puustinen, H. Jantunena, M. T. Sebastian, *J. Mater. Chem. C* **2015**, 3, 9240.

[51] J. Lim, J. Kim, Y. J. Yoon, H. Kim, H. G. Yoon, S. N. Lee, *Curr. Appl. Phys.* **2012**, 12, E14.

[52] C. Gautam, S. Chelliah, *RSC Adv.* **2021**, 11, 31284.

The table of contents entry and figure:

*Junjin Che, Cécile Zakri, Maxime Bronchy, Wilfrid Neri, Isabelle Ly, Philippe Poulin, Jinkai Yuan**

Inkjet Printing of All Aqueous Inks to Flexible Microcapacitors for High-Energy Storage

A flexible dielectric capacitor is inkjet printed based on all-aqueous functional inks including conductive carbon nanotube inks and dielectric polyvinylidene fluoride latex and boron nitride inks. The origin ink formulations coupled with printed heterostructures allows for a high energy storage density, which is superior to most of the state-of-the-art dielectrics printed from solvent-based formulations.